Many-body phases in Jaynes-Cummings-Hubbard arrays

Jin-Lou Ma,[1,*] Bobo Liu,[1,*] Qing Li,[2] Zexian Guo,[1] Lei Tan,[3,†] and Lei Ying[1,‡]

[1]*School of Physics, and Interdisciplinary Center for Quantum Information, Zhejiang University, Hangzhou 310027, China*

[2]*School of Jia Yang, Institute for Quantum Technology and Engineering Computing, Zhejiang Shuren University, Shaoxing, Zhejiang 312028, China*

[3]*Lanzhou Center for Theoretical Physics, Key Laboratory of Theoretical Physics of Gansu Province, Lanzhou University, Lanzhou, Gansu 730000, China*

(Received 23 August 2023; revised 15 December 2023; accepted 20 February 2024; published 11 March 2024)

Disorder in one-dimensional (1D) many-body systems facilitates abundant phases such as many-body localization (MBL) and thermalization. However, it remains unclear regarding their existence and behavior within hybrid quantum systems. Here, based on a simple bosonic-spin hybrid model, known as the Jaynes-Cummings-Hubbard (JCH) array, we investigate the effect of disorder compared to the phenomena in the clean system with the variation of atom-photon coupling strength. By using the level-spacing ratio, entanglement entropy, and the properties of observable diagonal and off-diagonal matrix elements, we find that strong disorder results in the appearance of a MBL phase in the JCH model that strongly violates the eigenstate thermalization hypothesis (ETH), while a conditional prethermal behavior can exist in the weak disorder regime. The conditional prethermal dynamics is based on the choice of initial product states. This work systematically reveals abundant many-body phases in the 1D JCH model and clarifies the discrepancies in the thermalization properties of systems with and without disorder.

DOI: 10.1103/PhysRevA.109.033707

I. INTRODUCTION

Many strongly correlated particles in a closed quantum system enable abundant interesting phases. In the past two decades, a large number of works have concluded that existence of strong disorder can strongly violate the eigenstate thermalization hypothesis (ETH) in one-dimensional (1D) nonintegrable many-body systems and a phase transition from thermalization to many-body localization (MBL) in various systems [1–3], which is an extension of Anderson localization in many-body systems [4,5]. The local integrals of motion lead to the system retaining information about its initial state for a long time in this dynamic phase [5–13]. The significance of studying such systems lies in the order of excited states in its entire energy spectrum [14–19], which were argued is potentially applied to the storage of quantum information [1,20].

The localization phase of many-body systems caused by disorder in a chain configuration for spins, fermions, or bosons has received extensive attention [21–36]. It can be asked whether such a MBL phase and its transition to thermalization can exist in a hybrid quantum many-body system, in which the Jaynes-Cummings-Hubbard (JCH) model is a typical example that has the advantages of precise manipulation, individual addressing, and the construction of any geometric structure [37]. The JCH model is a hybrid system of photons and spins, in which there are novel matter states and phenomena [37].

In this paper, we focus on the JCH model formed by a set of coupled cavities. Each cavity traps photons interacting with a two-level quantum system (it can be atom, qubit, or others) and this atom-photon interaction induces intrinsic nonlinear effect [38]. Such a model is a nonintegrable system [39,40], reminiscent of anyonic tight-binding quadratic models [41], which is different from the cross-stitch disordered lattice with a flat band [42]. For experimental platforms, disorder is inevitable. It is not yet clear how disorder affects the thermalization properties of the JCH model. Here, we choose the atom-photon interaction as the disordered quantity, induced by the random locations of the atom in cavities, as illustrated in Fig. 1. Thus, the disorder does not change the sign of the atom-cavity coupling strength, being in a range of $[0, D]$, where D is the maximum coupling strength. In this paper, we will unravel the veil of the influence of this kind of disorder on the thermal properties of the JCH chain and discuss its difference from a clean system. The lattice structure of the JCH model and the disorder introduced over the atom-photon interaction set it apart from conventional spin chain models. Intuitively, both weak and strong disorders in the JCH model could lead to distinct many-body dynamics. Note that our work is performed without losses, while losses are inevitable for any quantum optical system [43]. Thus, properly dealing with dissipation has to be considered in future study.

Here, through numerical simulation, we find that under the weak disorder strength related to atom-photon interactions, the system behaves in the quasi-integrable phase as if there was no disorder [44]. However, disorder actually leads to the

*These two authors contributed equally to this work.
†tanlei@lzu.edu.cn
‡leiying@zju.edu.cn

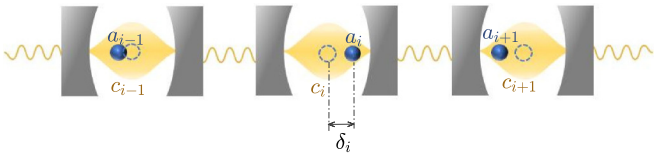

FIG. 1. Schematic diagram of the JCH array with coupling disorder. The 1D JCH model comprises interconnected Jaynes-Cummings models via photon tunneling (represented by yellow wavy curves), wherein each cavity accommodates a two-level atom (depicted by blue balls), which is randomly fixed at a position δ_i deviating from the central position of the cavity.

emergence of a prethermal time that depends on the initial state [45]. The quasi-integrable phase is a region close to the integrable point, which exhibits behavior similar to that of MBL under the finite size [44]. At the regime of medium disorder (coupling) strength, the ergodic phase appears in the disordered (clean) system. In this scenario, the system exhibits thermalized behavior, implying that over an extended period of evolution, the excitation population becomes homogeneously distributed throughout the system, regardless of its initial state. At strong coupling strength, accompanied by strong disorder, the system enters into a typical MBL phase, which has been validated by a large number of nonintegrable models, while in the clean system, there is an emergence of quasi-integrable phase. The paper is organized as follows. Section II presents the theoretical model and introduces level-spacing ratio and entanglement entropy to study the various phases of the disordered JCH system. We investigate the effect of disorder on phase transition in Sec. III. Section IV is devoted to discussion of the eigenstate thermalization of the disordered and the clean JCH systems.

II. DISORDERED AND CLEAN JAYNES-CUMMINGS-HUBBARD ARRAYS

We consider a disordered one-dimensional (1D) JCH model, and the schematic diagram of it is shown in Fig. 1 [46], whose Hamiltonian at the rotating wave approximation is given by ($\hbar = 1$)

$$H' = \sum_i^L [\omega_c a_i^\dagger a_i + \omega_a \sigma_i^+ \sigma_i^- + g_i(a_i\sigma_i^+ + a_i^\dagger \sigma_i^-)] - J\sum_i^{L-1}(a_i^\dagger a_{i+1} + a_i a_{i+1}^\dagger), \quad (1)$$

where the first two terms of the Hamiltonian describe free Hamiltonians of photons and the two-level system on each site, and ω_a (ω_c) is the frequency of the two-level system (photons) in single cavities. We only consider the resonance frequency case ($\omega_a = \omega_c$). σ_i^+ and σ_i^- are the atomic raising and lowering operators, respectively. Their corresponding commutation relations are $[\sigma_i^+, \sigma_j^-] = \delta_{ij}\sigma_i^z$. $a_i^\dagger$ (a_i) is the photon creation (annihilation) operator for the ith site. They satisfy commutative relationship $[a_i, a_j^\dagger] = \delta_{ij}$. L is the number of lattice sites. The atom-photon coupling strength is $g_i \in [0, D]$ for the ith cavity and D denotes the disorder strength [47]. The term in the second line is the sum of a hopping term of photons, and we assume that all the hopping strength of photons between the nearest neighboring cavities is identical and equal to J. This kind of nonintegrable Hamiltonian can exhibit thermalized and quantum chaotic behavior, distinguishing from integrable quadratic models [48]. By using the rotating transformation operator $U = \exp[i\sum_{j=1}^L \omega_c(a_j^\dagger a_j + \sigma_j^+\sigma_j^-)t]$, the Hamiltonian in Eq. (1) can be rewritten as

$$H = \sum_i^L g_i(a_i\sigma_i^+ + a_i^\dagger\sigma_i^-) - J\sum_i^{L-1}(a_i^\dagger a_{i+1} + a_i a_{i+1}^\dagger). \quad (2)$$

Numerical simulation in the rest of the content is based on Hamiltonian Eq. (2). In addition, the total number of atomic and photonic excitations is fixed as $N = \sum_i(a_i^\dagger a_i + \sigma_i^+\sigma_i^-) = \sum_i(n_i^c + n_i^a)$, and we consider the open boundary condition (OBC) where the filling factor is $\nu \equiv N/L = 1/2$. The disordered JCH model only has a chiral symmetry, and its corresponding chiral operator is [40] $\Gamma = \Pi_{j\in\text{even}} e^{i\pi a_j^\dagger a_j}\Pi_{j\in\text{odd}}\sigma_j^z$. Then, the dimension of Hilbert space of H is given by [40,49]

$$\mathcal{D} = \sum_{s=1}^N \frac{L(N+L-s-1)!}{(N-s)!(L-s)!s!}. \quad (3)$$

The basis vectors are written as $|\mathbf{n}\rangle \equiv \prod_i |n_i^c, n_i^a\rangle_i$. By utilizing the exact diagonalization, the maximum size of the system is $L = 10$.

In order to clarify the special behaviors of disorder, the results of the disordered JCH model are compared to those of the clean JCH model. The Hamiltonian of the clean JCH model is given by

$$H_{\text{cl}} = g_{\text{cl}}\sum_i^L(a_i\sigma_i^+ + a_i^\dagger\sigma_i^-) - J\sum_i^{L-1}(a_i^\dagger a_{i+1} + a_i a_{i+1}^\dagger). \quad (4)$$

The Hamiltonian H_{cl} owns the extra reflective symmetry. Under the reflection (parity) operator P, we study the clean JCH model in antisymmetric subspaces.

For the characterization of the MBL phase and ergodic phase, we need to introduce two physical quantities. The first one is the statistical features of spectrum by the level-spacing ratio $\langle r\rangle$ [50,51], which is a statistical quantity and is the average over $r_n = \min\{\Delta E_{n+1}/\Delta E_n, \Delta E_n/\Delta E_{n+1}\}$ with $\Delta E_n = E_{n+1} - E_n$ and E_n is the nth eigenenergy. For the MBL phase, the level-spacing ratio exhibits a Poisson distribution with $\langle r\rangle \approx 0.386$, while it shows the Wigner-Dyson distribution with $\langle r\rangle \approx 0.536$ in the ergodic phase [50,52,53]. In this paper, "$\langle\cdot\rangle$" indicates the average of physical quantities including eigenstates and disordered realizations. The other quantity is the half-chain entanglement entropy (EE) $S_{L/2} = -\text{Tr}[\rho_s \ln(\rho_s)]$ with $\rho_s = \text{Tr}_{i\leqslant L/2}[|n\rangle\langle n|]$. The EE describes how information spreads from one part of the system [1]. In the MBL phase, the average EE, $\langle S_{L/2}\rangle$, slowly grows as the time evolution and follows an area-law scaling [14,18,54]. Differently, $\langle S_{L/2}\rangle$ yields a volume-law scaling in the ergodic phase, which approaches to the Page value S_{P} for a random pure state [55]. To clearly describe the occurrence of MBL to ergodic phase transition, it is also necessary to show the sample-to-sample deviation of the half-chain EE ΔS, and its peak value represents the phase transition point [18,56,57].

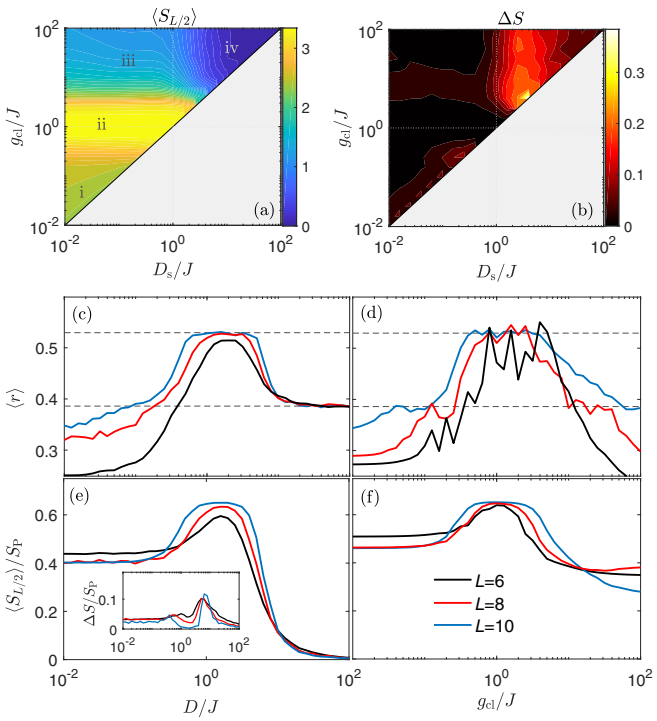

FIG. 2. (a) The EE $\langle S_{L/2}\rangle$ and (b) the sample-to-sample deviation of the EE ΔS as a function of g_{cl}/J and $D_s/J \in [D/2J, D/2J]$, respectively. Regions i and iii represent the quasi-integrable phase, region iv represents the MBL phase, and region ii represents the ergodic phase.. (c) The level-spacing ratio $\langle r\rangle$ and (e) the EE $\langle S_{L/2}\rangle/S_P$ as functions of the scaled disorder strength D/J in the disordered JCH model. The inset of (e) is the deviation of the EE $\Delta S/S_P$. The average half-chain EE is rescaled by the Page value S_P. (d) The level-spacing ratio $\langle r\rangle$ as a function of the scaled coupling strength g_{cl}/J in the clean JCH model. The EE $\langle S_{L/2}\rangle/S_P$ as a function of the scaled coupling strength g_{cl}/J in (f). Gray dashed lines mark $\langle r\rangle = 0.386$ (Poisson distribution) and 0.536 (Wigner-Dyson distribution) in (c) and (d). In the clean JCH model, the photon-atom coupling strength g_{cl} of each on site is assumed to be the same. The averaged physical quantities of the disordered JCH model are taken by 1000, 400, and 50 disordered samples for $L = 6$, 8, and 10.

III. MANY-BODY PHASES AND TRANSITIONS

We set out to the responses of the level-spacing ratio $\langle r\rangle$ and the average half-chain EE of the disordered (clean) model with increasing the disorder strength D/J (the pristine photon-atom coupling strength g_{cl}/J). In order to improve the efficiency of numerical calculations, the middle third of the energy spectrum was selected. Figures 2(a) and 2(b) depict the average half-chain EE, $\langle S_{L/2}\rangle$, and its deviation, denoted as ΔS, respectively, as a function of the coupling strength $g_{cl/J}$ and disorder strength D_s/J. Here, we consider a generalized model with random atom-photon coupling $g_{cl}/J - D_s/J \leqslant g_i/J \leqslant g_{cl}/J + D_s/J$ in a general point $(D_s/J, g_{cl}/J)$ of the diagram. Then, $(D_s/J = 0, g_{cl}/J)$ corresponds to the clean case [absent in Figs. 2(a) and 2(b) as D_s/J is in the logarithmic scale], while $(D_s/J = D/2J, g_{cl} = D/2J)$ corresponds to the disordered case. There are three many-body phases in the disordered JCH model, i.e., quasi-integrable (i and iii), MBL (iv), and ergodic phases (ii). In Figs. 2(c)–2(f), as the disorder strength increases, the level-spacing ratio exhibits a range of distributions, transitioning from the quasi-degenerate distribution to the Wigner-Dyson distribution, and finally converging to the Poisson distribution. Similarly, the EE undergoes a transition from an area-law, then a volume-law behavior, to an area-law behavior eventually. Here, we notice that the quasi-degenerate distribution indicates that there is a significant amount of near degeneracy in the eigenenergy spectrum of the Hamiltonian. As the system size increases, the quasi-degenerate distribution of energy-level spacing approaches the Poisson distribution, and the level-spacing ratio $\langle r\rangle$ trends to be 0.386 as shown in Figs. 2(c) and 2(d). Upon the analysis of entropy, as the system size increases, the half-chain EE gradually approaches a small constant value (<1) with weak disorder strength. This implies that the EE obeys the area law at the thermodynamic limit and the variation of EE is a finite-size effect in Figs. 2(d) and 2(e). However, for strong disorder strengths, the finite-size effect is almost negligible. As for the clean JCH model, these two quantities exhibit similarities to those of the disordered JCH model in the regime of weak and intermediate coupling strengths, whereas for strong coupling interactions without disorder, the finite-size effect is relatively pronounced.

We also show the sample-to-sample deviation of the EE $\Delta S/S_P$ for the disordered JCH model in the inset of Fig. 2(e). The enhancement of the peak value of $\Delta S/S_P$ at $D/J \sim 6.3$ is at larger system size $L = 10$, implying that the system shows an ergodic-MBL phase. Note that the other peak approaches to the weak disorder strength ($D/J \sim 10^{-1}$) with the increase of size L. Thus, we suppose that, under the weak disorder limit, the disordered system presents the same integrable behaviors as for the clean system [49]. Based on the above results, it can be concluded that the intermediate disorder displays an ergodic phase.

Next, we show the dynamics of the average half-chain EE for different many-body phases in the disordered and the clean JCH model. Previous works indicate that the EE dynamics shows a scaling behavior of log$t$ for the MBL phase [58,59], while the EE rapidly tends to a saturation value in the ergodic phase [60]. Here, Fig. 3 shows the time evolution of the EE under different parameters, where the initial state is chosen as $|\mathbf{n}\rangle_{in} \equiv \prod_{i\in odd} |1, g\rangle_i \otimes \prod_{j\in even} |0, g\rangle_j$. In Fig. 3(a), we can find that at a disorder strength of $D/J = 0.01$, its EE exhibits a rapid increase at early time, followed by oscillations, a metastable period, and eventually approaches a saturation value slowly. One can find that the time-average values of $\langle S_{L/2}(t)\rangle$ for oscillating and metastable period regimes are almost identical. It can be seen from Fig. 3(a) that the phenomena of oscillation and metastable period remain stable across different system sizes. As the number of disordered samples increase, the oscillating period tends to become invariant and the metastable period becomes a smooth function [see details in Fig. 9(a) of Appendix A]. This observation suggests that oscillation is an inherent characteristic of the weak disorder system, while the average behavior of disordered realizations gives rise to a metastable period in the finite-size system. In addition, in the disorder-free case with a small coupling $g_{cl}/J = 0.01$, the EE dynamics show similar phenomena to the weak disorder case, while the phenomenon of metastable period disappears, as shown in Fig. 3(b). The observed

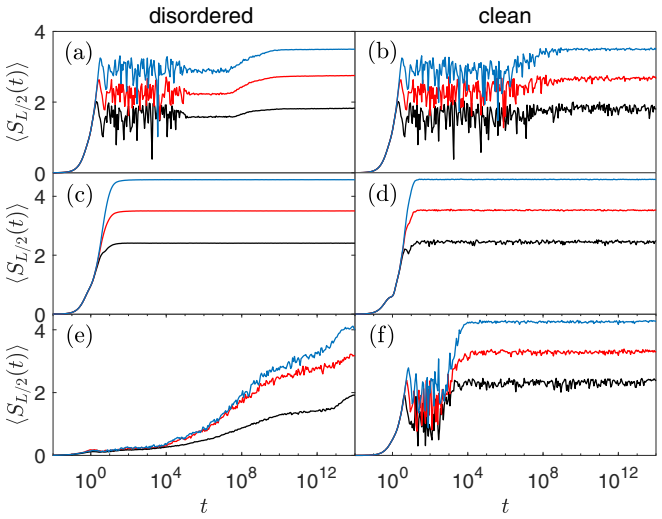

FIG. 3. The average half-chain EE $\langle S_{L/2}(t)\rangle$ vs time t for the disordered (right) and the clean (left) JCH model. Three colors represent three sizes $L = 6$ (black), 8 (red), and 10 (blue). The top, middle, and bottom figures correspond to D/J, $g_{\rm cl}/J = 0.01$, 2, and 100, respectively. The averaged physical quantities of the disordered JCH model are taken by 1000, 400, and 100 disordered samples for $L = 6$, 8, and 10. Note that we plot the average time evolution of $3\langle S_{L/2}(t)\rangle$ in (e).

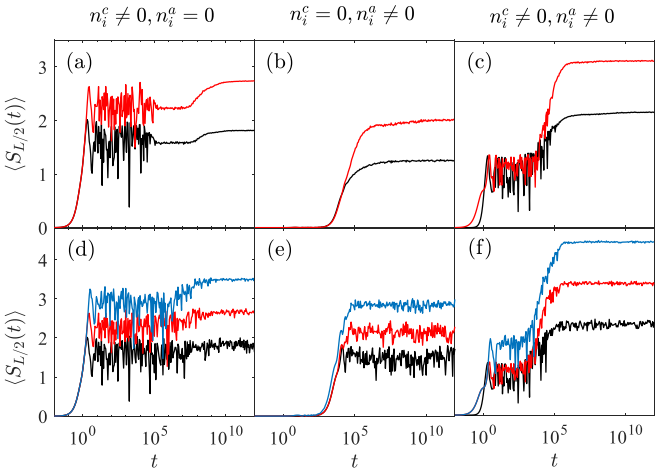

FIG. 4. The average half-chain EE $\langle S_{L/2}(t)\rangle$ vs time t for the disordered (first column) and the clean (second colum) JCH model with different initial states. The disordered and clean cases correspond to D/J and $g_{\rm cl}/J = 0.01$, respectively. (a) and (d) are shown by the initial state ($N^c \neq 0$, $N^a = 0$). (b) and (e) are shown by the initial state ($N^c \neq 0$, $N^a \neq 0$). (c) and (f) are shown by the initial state ($N^c = 0$, $N^a \neq 0$). N^c (N^a) is the number of photonic (atomic) excitations. The black, red, and blue lines represent sizes $L = 6$, 8, and 10, respectively. The 1000 (100) disordered samples correspond to $L = 6$ (8) for the disordered case.

difference can be interpreted as an indication that weak disorder strength induces prethermalization during the metastable periods [60–62].

When D/J, $g_{\rm cl}/J = 2$, both disordered and clean cases are in ergodic phases, and the EE tends to reach saturation rapidly. In the disordered system at $D/J = 100$ [Fig. 3(e)], the EE $\langle S_{L/2}(t)\rangle$ exhibits a $\log(t)$ scaling behavior before reaching a saturation value, while for the clean system at $g_{\rm cl}/J = 100$ [Fig. 3(f)], the results are similar to the case of $g_{\rm cl}/J = 0.01$. The difference lies in the fact that the latter one has a prolonged oscillating period for the certain initial states and ultimately reaches a saturation value rapidly within the finite-size system. It is noteworthy that the dynamics of the EE differ significantly between the disordered and clean coupling under strong interactions. For the moment, we roughly consider that the weak D/J, $g_{\rm cl}/J$ and the strong $g_{\rm cl}$ are quasi-integrable phases, the intermediate regime of D/J and $g_{\rm cl}/J$ are ergodic phases, and the strong D/J is a MBL phase.

Furthermore, we find that the emergence of prethermal dynamics strongly depends on initial states at the weak disorder regime, say, $D/J = 0.01$, as shown as the EE dynamics in Figs. 4(a)–4(c). The prethermal dynamics occurs for the initial states only with photonic excitations. On the contrary, the EE would rapidly grow after a long threshold time for the initial states only with atomic excitations. If the initial state consists of both atomic and photonic excitations, the dynamics of half-chain EE only show the oscillating period. Differently, as for the clean case of the coupling strength $g_{\rm cl}/J = 0.01$ in Figs. 4(d)–4(f), there is no metastable prethermalization process and the thermal plateau is higher than the case of initial states with only atomic excitations.

To better exhibit the influence of initial states, we show the dynamics of occupation numbers of all sites for three kinds of initial states at weak atom-cavity coupling $D/J = g_{\rm cl}/J = 0.01$ in Fig. 5. The whole JCH system is consisting of atomic and photonic parts. For the initial state only with photonic excitations and before reaching the maximum half-chain EE, the populations are constrained in the photonic part, exhibiting a prethermal dynamics, distinguishing from the case of the clean system ($g_{\rm cl}/J = 0.01$) with a nonthermal dynamics, as shown in Figs. 5(a) and 5(d). This means that this weak coupling prevents energy exchange between atoms and photons within a considerable amount of time, while the weak disorder causes a metastable prethermalization before the weak energy exchange between atoms and photons. The atoms are nearly decoupled from the photons. Thus, the atomic excitations that are occupied are nearly stuck for a long time of the order of $1/g_{\rm cl}$ ($1/D$). This provides the metastable atomic states which are nearly degenerate as there is no hopping between atoms. Therefore, the populations stay at the atomic part, showing a metastable dynamics in both cases of disordered and clean systems in Figs. 5(b) and 5(e). Also, the local nature of these atomic modes restricts EE and shows the area law. Thus, there is only weak indirect interatomic hopping and, as a result, no remarkable oscillations appear in the dynamics, as shown in Figs. 4(b) and 4(e). Unlike that, for the initial states with both atomic and photonic excitations, both atomic and photonic parts exhibit thermal-like dynamics, implying larger entanglement entropy than the case of the initial states only with photonic excitations.

IV. EIGENSTATE THERMALIZATION PROPERTIES

To further investigate the entire system properties, in this section, we analyze the thermalization of the disordered and clean JCH model to examine the validity of the ETH in

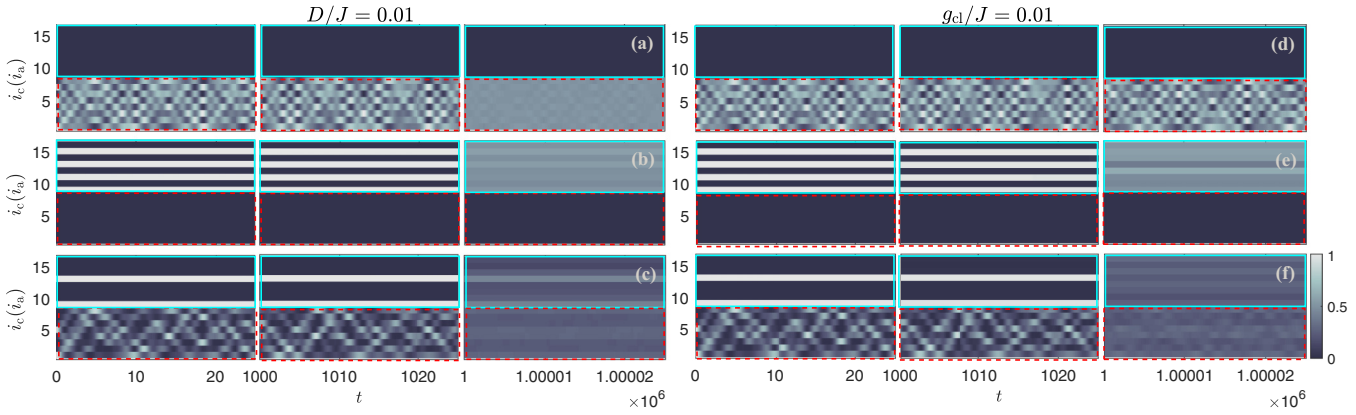

FIG. 5. The averaged atomic (photonic) excitations occupation occupancy per site $\langle n_i^a \rangle$ ($\langle n_i^a \rangle$) as a function of time t with different initial states for the disordered and clean JCH models. The initial state of (a) and (d) is $\prod_{i\in\text{odd}} |1, g\rangle_i \otimes \prod_{j\in\text{even}} |0, g\rangle_j$, the initial state of (b) and (e) is $\prod_{i\in\text{odd}} |0, e\rangle_i \otimes \prod_{j\in\text{even}} |0, g\rangle_j$, and the initial state of (c) and (f) is $|1, e\rangle_1 \otimes |1, e\rangle_5 \otimes \prod_{j\in\text{others}} |0, g\rangle_j$. The site index of photonic (atomic) excitations is 1–8 (9–16). Each initial state exhibits three periods of time evolution, namely, $0 \leqslant t_1 < 25$, $1000 \leqslant t_2 < 1025$, and $10^6 \leqslant t_3 < 1.000\,025 \times 10^6$. The disordered and clean cases correspond to D/J and $g_{cl}/J = 0.01$, respectively. The system size is chosen by $L = 8$. The averaged physical quantities of the disordered JCH model are taken by 100 disordered samples.

different many-body phases, which were studied by the EE dynamics above. In order to determine whether the system can be thermalized, it is necessary to pay attention to whether the diagonal and nondiagonal elements of the local observable operator O satisfy the ETH [63–66]. The definition of local operator is written as

$$O_{nm} = O(\bar{E})\Delta E_{nm} + e^{-S(\bar{E})/2} f_O(\bar{E}, \omega') R_{nm}, \tag{5}$$

where $\bar{E} = (E_n + E_m)/2$ is the average energy of adjacent eigenenergies, and $\omega' = E_n - E_m$ is its energy difference. Here, n and m are the indices of eigenstates, $S(\bar{E})_{\text{th}}$ stands for the thermodynamic entropy, and R_{nm} is the random variable which obeys a normal distribution. In the thermodynamic limit, $O(\bar{E})$ and $f(\omega', \bar{E})$ are smooth functions about ω' and $\bar{E}$. The first term in Eq. (5) is the expected values of the observable and the second term describes the off-diagonal matrix elements. The average eigenstate-to-eigenstate fluctuations of diagonal expectation is given by [29]

$$\overline{|\delta O_{nn}|} = \overline{|O_{n+1,n+1}| - |O_{n,n}|}. \tag{6}$$

In general, the eigenstate-to-eigenstate fluctuations both for diagonal and off-diagonal elements exponentially decay as the system size increases if the system satisfies the ETH [25–30,67]. Here, we select two specific local observables to discuss whether their behaviors are consistent with the predictions of the ETH. The first observable is the occupancy operator $N_{L/2}$ at the site $L/2$, while the second observable is the kinetic operator per site $H_{\text{kin}} = (1/L)\sum_i^{L-1}(a_i^\dagger a_{i+1} + a_i a_{i+1}^\dagger)$, which represents the reduced photon hopping term.

Firstly, the diagonal elements of observable $N_{L/2}$ and H_{kin} as functions of the energy density are plotted in Fig. 6. The energy density is defined by $\epsilon_n = (E_n - E_{\min})/(E_{\max} - E_{\min})$, where E_n is the n-th eigenenergy, and $E_{\min}(E_{\max})$ represents the minimum (maximum) eigenenergies. Here, we focus on the middle four-fifths of the energy spectrum. In Figs. 6(a), 6(b), 6(g), and 6(h), it can be seen that at disorder strength $D/J = 0.01$ and coupling strength $g_{cl}/J = 0.01$, the fluctuations of the disordered and clean cases do not diminish with increasing system size L for both the observables $N_{L/2}$ and H_{kin}. For the observable H_{kin}, whether it is the disordered or clean case, we find that with the increase of energy density ϵ_n, the expected value changes linearly with minor fluctuation. The result indicates that the atom-photon coupling term acts as a small perturbation, and the hopping term of the photon and the Hamiltonian H of Eq. (2) can be regarded as commutative. This implies that the observable H_{kin} and the Hamiltonian in Eq. (2) share almost identical eigenvalues and eigenstates. Therefore, H_{kin} is a linear function of the energy density ϵ_n. Thus, H_{kin} cannot be simply considered as a local observable to diagnose the thermalization. At a mediate disorder strength, say, $D/J = 2$, the fluctuations of the observable $N_{L/2}$ decrease as the size L increases. But, the observable H_{kin} is almost a smooth function of energy density ϵ_n, even in small system sizes. The behavior of the clean system ($g_{cl}/J = 2$) is consistent with that of the disordered system. Also, we can see this phenomenon from the average eigenstate-to-eigenstate fluctuations $\overline{|\delta O_{nn}|}$ of diagonal elements decreasing exponentially fast with increasing L in Figs. 7(a) and 7(b) for ergodic phases in the disordered and clean systems. Because the Hilbert-Schmidt norm of operator H_{kin} scales as $1/\sqrt{L}$ [36,67], the average eigenstate-to-eigenstate fluctuations of H_{kin} are $\propto (L\mathcal{D})^{-1/2}$. In the case of D/J, $g_{cl}/J = 100$, although the fluctuations of the two observables increase with the increase of system size for two kinds of systems, it is remarkable that the diagonal elements of disordered and clean systems change differently with energy densities. Specifically, the expected values of the observables show a uniform distribution for disordered systems. while for the clean system, there is a large amount of quasi-degeneracy in the energy densities, resembling the separation of energy bands. In short, by comparing the distributions of diagonal elements between disordered and clean systems, we find that the fluctuations in the disordered case are noticeably smaller, in particular, in the ergodic phases (D/J, $g_{cl}/J = 2$). This discrepancy can be attributed to the averaging effect of the disordered samples.

Based on Figs. 6 and 7, we can conclude that D/J, $g_{cl}/J = 2$ (ergodic phase) meets ETH, while $D/J = 0.01$, $g_{cl}/J =$

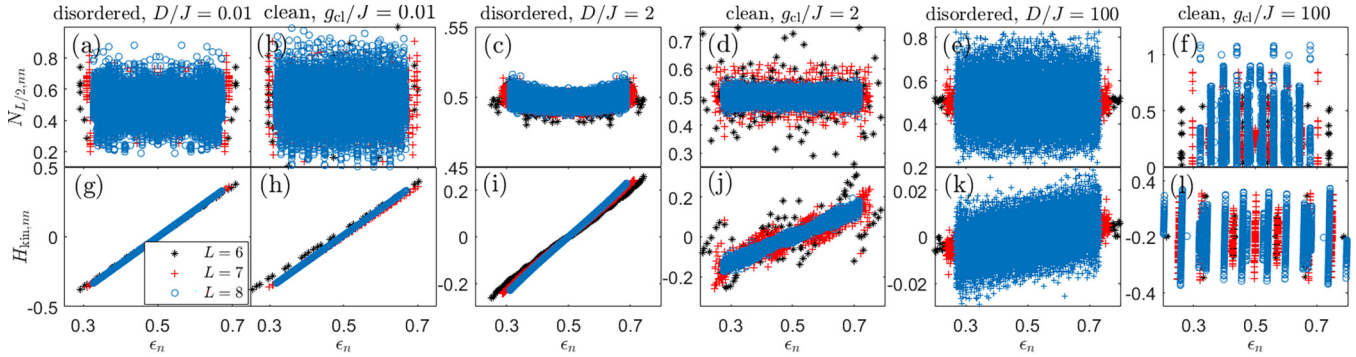

FIG. 6. The diagonal matrix elements of [(a)–(f)] $N_{L/2}$ and [(g)–(l)] H_{kin} as a function of the energy density ϵ_n with different D/J and g_{cl}/J for the disordered and clean JCH models. The black star, red plus, and blue circle lines correspond to $L = 6$, 8, and 10, respectively. The averaged physical quantities of the disordered JCH model are taken by 1000, 400, and 100 disordered samples for $L = 6$, 8, and 10, respectively.

0.01, 100 (quasi-integrable phase) and $D/J = 100$ (MBL phase) strongly violate ETH. We also find that the average disordered diagonal elements of $N_{L/2}$ and H_{kin} are symmetrical about the axis of $\epsilon_n = 0.5$ and the point $(\epsilon_n, H_{kin,nn}) = (0.5, 0)$, respectively. This symmetry arises due to the commutation relation $[\Gamma, N_{L/2}] = 0$, which leads to $\langle n|N_{L/2}|n\rangle = \langle n|\Gamma^\dagger N_{L/2}\Gamma|n\rangle$. In addition, the anticommutation relation $\{\Gamma, H_{kin}\} = 0$ results in $\langle n|H_{kin}|n\rangle = -\langle n|\Gamma^\dagger H_{kin}\Gamma|n\rangle$ [40]. Differently, the diagonal elements of the clean JCH model are not symmetrical since the excitation number N is odd. According to the symmetry analysis in Appendix B, when the chiral operator Γ and the reflection operator P commute, the system has chiral symmetry in the antisymmetric subspace with reflective symmetry for the even excitation number N. However, when the operators Γ and P do not commute, there is no such chiral symmetry in the antisymmetric subspace for the odd excitation number N. For the disordered system, the reflection symmetry is lost, thus chiral symmetry emerges in the systems both with odd and even excitations.

Here, we focus on the variance of the off-diagonal elements. In our model, the variance $|\overline{O_{nm}}^2 - |\overline{O_{nm}}|^2| \approx \overline{|O_{nm}|^2}$ since observables $\overline{H_{kin,nm}} \approx 0$ and $\overline{N_{L/2,nm}} \approx 0$, the same as in spin systems [67–69]. Also, $\overline{|O_{nm}|^2}$ is a quantity to study fluctuation dissipation relation [31], transport properties [27,70], periodic driven heating rate [71], etc. In Fig. 8, we plot the coarse-grained average scaled variances $\overline{|H_{kin,nm}|^2}$ and $\overline{|N_{L/2,nm}|^2}$ of the off-diagonal matrix elements with $\omega = \epsilon_n - \epsilon_m$. For D/J, $g_{cl}/J = 0.01$, the properties of the two systems are similar: both of them have a strong dispersion. At disorder strength $D/J = 2$ and coupling strength $g_{cl}/J = 2$, the coarse-grained averages $\overline{|H_{kin,nm}|^2}$ and $\overline{|N_{L/2,nm}|^2}$ of the off-diagonal matrix elements show smoothing functions of ω. The variance of off-diagonal matrix elements satisfies $\overline{|O_{nm}|^2} \propto (L\mathcal{D})^{-1}$ [36,67]. The difference in scaling behaviors of the two observables can be attributed to the Hilbert-Schmidt norms of the observable H_{kin}, whose scaling behaviors are given by $\sim 1/\sqrt{L}$. On the other hand, the off-diagonal matrix elements of the observables have similar behaviors in the disordered and clean systems. At strong disorder and strength coupling regimes, say, D/J, $g_{cl}/J = 100$, the variances of two observables are the smooth functions of ω for the disordered systems, but not for clean systems. In the clean system, the behavior is similar to the case at weak coupling strength (g_{cl}/J). In Fig. 8, we have that the variances of the observables for $L = 8$ and $L = 10$ show minimal finite-size effects in both the ergodic and MBL phases.

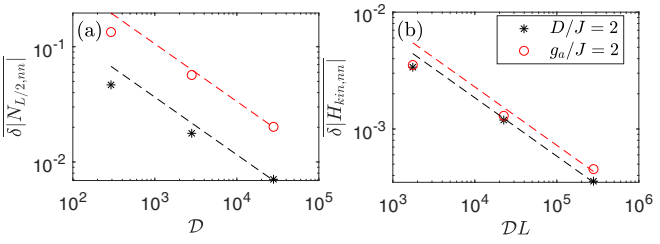

FIG. 7. Scaling of (a) $\overline{|\delta N_{L/2,nn}|}$ and (b) $\overline{|\delta H_{kin,nn}|}$ at the nonintegrable point of the disordered ($D/J = 2$) and the clean ($g_{cl}/J = 2$) JCH model. The dashed lines denote a power law scaling of $\propto x^{-1/2}$ in Figs. 7(a) and 7(b). The average physical quantities of the disordered JCH model are taken by 1000, 400, and 100 disordered samples for $L = 6$, 8, and 10, respectively.

The scaled variances of the off-diagonal matrix elements in the low-frequency ω part are briefly discussed below for the ergodic and MBL phases. Observables $N_{L/2}$ and H_{kin} exhibit data collapse as $L\omega$ decrease for different system sizes (see the insets of Fig. 8). For the ergodic phases (D/J, $g_{cl}/J = 2$), the collapse degrades as $L\omega$ increases and two variances of observables have a high value as $L\omega$ approaches to zero, indicating the diffusive dynamics, the same as with quantum-chaotic systems [63]. In addition, for the MBL phases ($D/J = 100$) with a large size, the variance of observable $N_{L/2}$ does not vanish as $L\omega$ approaches zero, while the observable H_{kin} approaches zero. This phenomenon is similar to the integrable XXZ chain [69]. By comparing Figs. 8(c), 8(d), and 8(e), we find that the variance of observable $N_{L/2}$ has the same behavior in the low-frequency regime for both the ergodic and MBL phases. This implies that the scaling behavior of observable $N_{L/2}$ is stable in ergodic and MBL phases. However, as the relationship between the variances of the observables and the frequency ω is not a smooth function in other cases, we will not discuss it in depth.

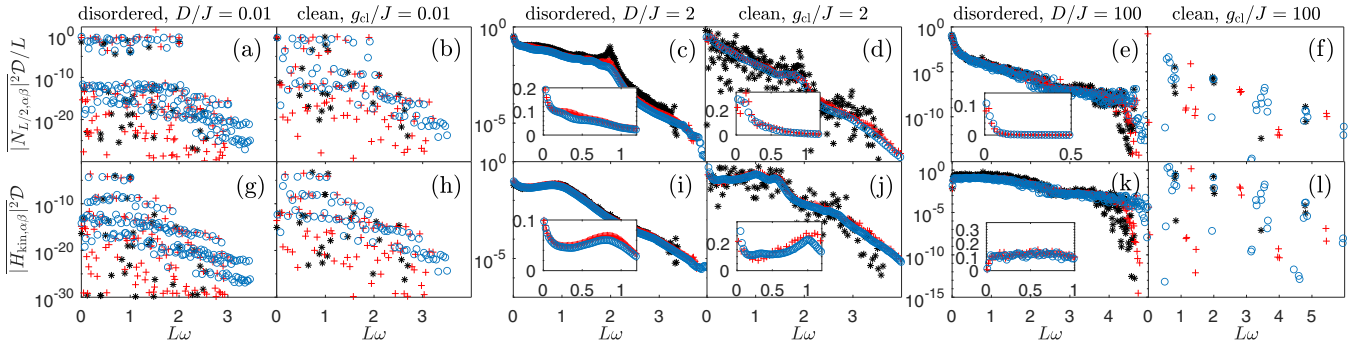

FIG. 8. [(a)–(f)] Coarse-grained averages of $N_{L/2}$ as a function of $L\omega$ with different D/J and $g_{\rm cl}/J$ for the disordered and clean JCH models. [(g)–(l)] Coarse-grained averages of $H_{\rm kin}$ as a function of $L\omega$ with different D/J and $g_{\rm cl}/J$ for the disordered and clean JCH models. The matrix elements are computed within a small window of energy around the average spectrum $\bar{\epsilon}$ of width 0.01ω. The averages in ω are calculated in windows with $\delta\omega = 0.002$. The black star, red plus, and blue circle lines correspond to $L = 6$, 8, and 10, respectively. The averaged physical quantities of the disordered JCH model are taken by 1000, 400, and 100 disordered samples for $L = 6$, 8, and 10, respectively.

To study the normality of distribution of the off-diagonal matrix elements, we calculate the ratio [67]

$$\Gamma_O(\omega) = \overline{|O_{n,m}|^2}/\overline{|O_{n,m}|}^2. \tag{7}$$

If the local observable operator $O_{n,m}$ has a normal distribution with a zero mean value, we have $\Gamma_O(\omega) = \pi/2$. The ratio $\Gamma_O(\omega)$ can identify the occurrence of eigenstate thermalization [67–69,72,73]. In Fig. 9, we present the results of $\Gamma_{N_{L/2}}(\omega)$ and $\Gamma_{H_{\rm kin}}(\omega)$ vs $L\omega$ in the eigenstates for the disordered and clean JCH models with different atom-photon coupling strengths. For $D/J = 0.01$ and $g_{\rm cl}/J = 0.01$, one can find that the $\Gamma_O(\omega)$ of two observables fail to collapse, in particular, in the case of large system sizes, meaning that the off-diagonal matrix elements of $N_{L/2}$ and $H_{\rm kin}$ do not obey the normal distribution. From Figs. 9(c), 9(d), 9(i), and 9(j), we find that $\Gamma_{N_{L/2}}(\omega)$ and $\Gamma_{H_{\rm kin}}(\omega)$ converge to $\pi/2$ with increasing system size for the ergodic regime of both the disordered ($D/J = 2$) and clean ($g_{\rm cl}/J = 2$) systems. We consider that the ratios at the small ω regime have a value close to $\pi/2$. As for $D/J = 100$ in Figs. 9(e) and 9(k), we find that the behaviors of both $\Gamma_{N_{L/2}}(\omega)$ and $\Gamma_{H_{\rm kin}}(\omega)$ depend on the system size and do not follow a normal distribution. In addition, the clean system $g_{\rm cl}/J = 100$ [Figs. 9(f) and 9(l)] exhibits a similar behavior with the case of $g_{\rm cl}/J = 0.01$. Neither of these cases exhibits a normal distribution, and the functions about $L\omega$ are not smooth.

Our analysis clearly demonstrates that the region exhibiting quasi-integrable behavior deviates from the ETH, while the ergodic region adheres to the ETH. However, the MBL region remarkably violates ETH and its behavior is consistent with that of integrable systems [67–69,73].

V. CONCLUSION

In this paper, the behaviors of 1D disordered and clean JCH systems, focusing on their quasi-integrable, ergodic, and MBL phases, are investigated. We explore the similarities and differences between quasi-integrable and MBL phases. Interestingly, we find that the prethermalization is remarkably dependent on its initial state at the weak disorder regime.

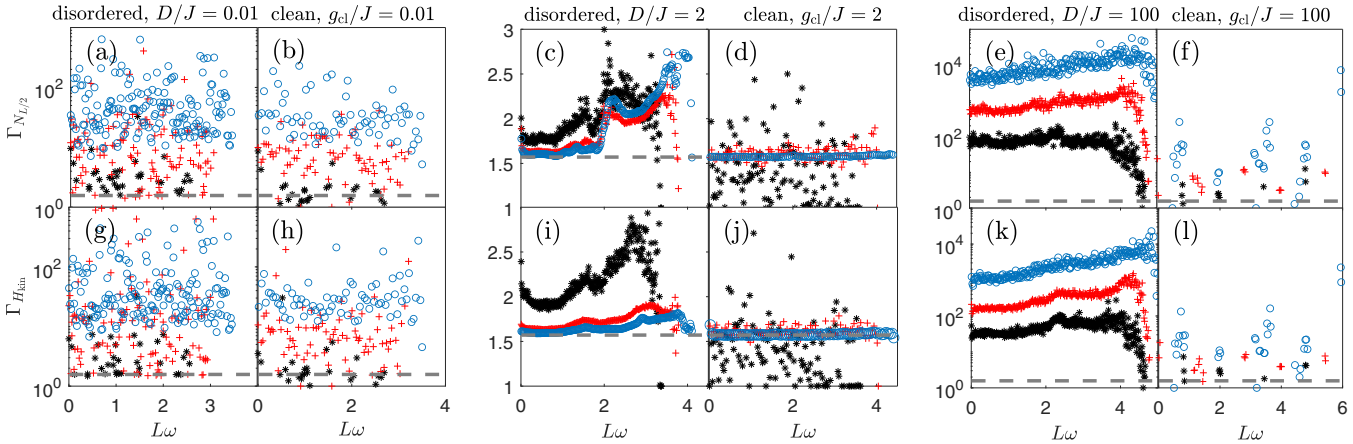

FIG. 9. The ratio $\Gamma_O(\omega)$ [(a)–(f)] for the occupancy operator $N_{L/2}$ and [(g)–(l)] for the kinetic operator $H_{\rm kin}$ as a function of $L\omega$ in the disordered and clean JCH models. The horizontal gray-dashed lines mark $\pi/2$ in all subgraphs. The matrix elements are computed within a small window of energy around the average spectrum $\bar{\epsilon}$ of width 0.01ω. The averages in ω are calculated in windows with $\delta\omega = 0.002$. The black star, red plus, and blue circle lines correspond to $L = 6$, 8, and 10, respectively. The averaged physical quantities of the disordered JCH model are taken by 1000, 400, and 100 disordered samples for $L = 6$, 8, and 10, respectively.

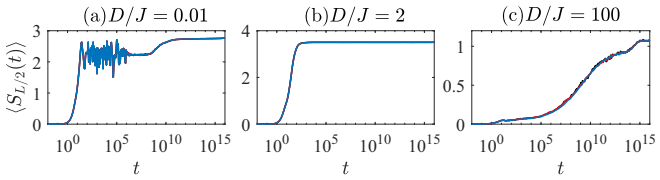

FIG. 10. The average half-chain EE $\langle S_{L/2}(t)\rangle$ vs time t for the disordered JCH model with different disorder strengths. Three colors represent three disordered samples [400 (black), 1000 (red), and 2000 (blue)] for sizes $L = 8$.

Regarding the ergodic phases, we observe that disorder has minimal impact on the system behavior at the regime where disorder strength is not strong enough, which is the expected result. However, for strong disorder strength, the system exhibits a MBL phase, with the same phenomena shown in other disordered systems. Furthermore, we also find that the JCH model in the MBL phase displays nonthermalization behaviors. The quasi-integrable phases also deviate the ETH. However, due to the presence of numerous quasi-degenerate energy levels, the matrix element behaviors of observables exhibit distinct characteristics compared to the conventional MBL phase, with a relatively discrete distribution. In summary, through a comprehensive analysis of 1D disordered and clean JCH systems, we have provided insights into the impact of disorder on MBL and prethermalization phenomena in these systems.

ACKNOWLEDGMENTS

This work was supported by the National Natural Science Foundation of China (Grant No. 12375021) and the National Key R&D Program of China under Grant No. 2022YFA1404203. Support was also provided by the Supercomputing Center of Lanzhou University.

APPENDIX A: THE EFFECT OF DISORDER SAMPLES

Here, in order to explain that different disordered samples make no difference on the system results, we compare the differences between the physical quantities under multiple disordered samples.

From Fig. 10, we can find that as the number of disorder samples increases, the behavior of the average half-chain EE $\langle S_{L/2}(t)\rangle$ becomes progressively smoother over time t. However, it is important to note that different disordered samples do not impact the oscillation region when the disorder strength is $D/J = 0.01$. In essence, the presence of additional disordered samples does not affect the behavior of the half-chain EE, except for its fluctuations.

It can be seen from Fig. 11 that when the disorder strength $D/J = 0.01$, the disorder samples have minimal impact on the diagonal elements of the observables. When the disorder strength $D/J = 2$, with the increase of the number of disorder samples, the fluctuations of the observable $N_{L/2}$ decrease gradually. However, the observable H_{kin} remains unchanged since there are negligible fluctuations in H_{kin} as a function of the energy density ϵ_n. In addition, when the disorder strength $D/J = 100$, the fluctuations of both observables decrease with

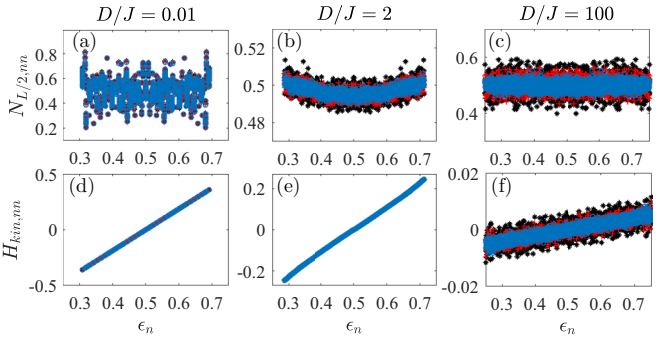

FIG. 11. The diagonal matrix elements of [(a)–(c)] $N_{L/2}$ and [(d)–(f)] H_{kin} as a function of the energy density ϵ_n with different D/J for the disordered JCH model. The black star, red plus, and blue circle lines correspond to 400, 1000, and 2000 disordered samples, respectively. The system size is chosen as $L = 8$.

the increase of the disordered samples. On the whole, the fluctuations of the diagonal elements of the observable H_{kin} are smaller than that of the observable $N_{L/2}$.

By choosing the same disordered samples in Fig. 12, one can easily find whether the changes of the diagonal element with sizes satisfy ETH under different disorder strengths.

Regarding the off-diagonal elements of the observables, the number of disordered samples also hardly affect the case of $D/J = 0.01$. However, for the other two cases, increasing the number of disordered samples leads to a reduction in fluctuations, resulting in smoother functions, as shown in Fig. 13. The influence of the disordered samples on the observable H_{kin} (not show here) has the same behaviors as that of $N_{L/2}$.

APPENDIX B: THE ANALYSIS OF CHIRAL SYMMETRY

In the clean case, chiral symmetry exists only in the case of even excitations for the antisymmetric subspace. Let us prove the reason for this phenomenon below. First, we consider the case where the number of excitations is even ($N \in$ even). The number of photons (atoms) defining the sum of odd lattice points and even lattice points is $\sum_{i\in\text{even}}^{L}(n_i^{\text{c}} + n_{i+1}^{\text{c}}) = N_{\text{e}}^{\text{c}} + N_{\text{o}}^{\text{c}} = N^{\text{c}}$ ($\sum_{i\in\text{even}}^{L}(n_i^{\text{a}} + n_{i+1}^{\text{a}}) = N_{\text{e}}^{\text{a}} + N_{\text{o}}^{\text{a}} = N^{\text{a}}$), where subscript "o" represents odd lattice points and subscript "e" represents even lattice points. At the same time, we also define

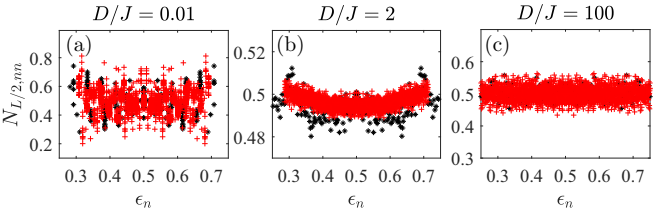

FIG. 12. The diagonal matrix elements of $N_{L/2}$ as a function of the energy density ϵ_n with different D/J for the disordered JCH model. The black star and red plus lines correspond to the system size $L = 6$ and 8, respectively. The disordered sample is chosen as 1000.

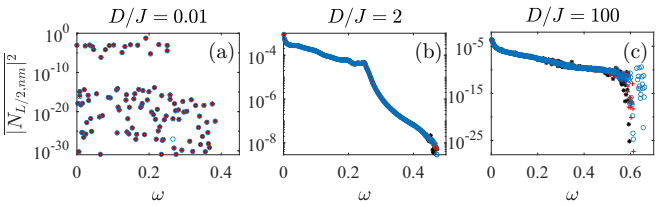

FIG. 13. Coarse-grained averages of $N_{L/2}$ as a function of ω with different D/J for the disordered JCH model. The matrix elements are computed within a small window of energies around the average spectrum $\bar{\epsilon}$ of width 0.01ω. The averages in ω are calculated in windows with $\delta\omega = 0.002$. The black star, red plus, and blue circle lines correspond to 400, 1000, and 2000 disordered samples, respectively. The system size is $L = 8$.

the following two quantities: $N_{\rm e}^{\rm c} + N_{\rm o}^{\rm a} = N_1$ and $N_{\rm o}^{\rm c} + N_{\rm e}^{\rm a} = N_2$.

For $N_1 + N_2 = N \in$ even, then

$$\begin{matrix} N_1 \in \text{even}, \\ N_2 \in \text{even}, \end{matrix} \quad \text{or} \quad \begin{matrix} N_1 \in \text{odd}, \\ N_2 \in \text{odd}. \end{matrix}$$

When $N_1 \in$ even, $N_{\rm e}^{\rm c} \in$ odd, and $N_{\rm o}^{\rm a} \in$ odd, since the relation $L = 2N$, the number of atomic ground states is $N - N_{\rm o}^{\rm a}$ (odd) for the odd number of lattice sites. Thus, $\Gamma|\mathbf{n}\rangle = e^{i\pi N_{\rm e}^{\rm c}}(-1)^{N-N_{\rm o}^{\rm a}} \prod_i |n_i^{\rm c}, n_i^{\rm a}\rangle_i = |\mathbf{n}\rangle$. When $N_1 \in$ even, $N_{\rm e}^{\rm c} \in$ even, and $N_{\rm o}^{\rm a} \in$ even, we can also get $\Gamma|\mathbf{n}\rangle = |\mathbf{n}\rangle$.

For the reflective symmetric state $P|\mathbf{n}\rangle = |\mathbf{n}'\rangle = |n_L^{\rm c}, n_L^{\rm a}\rangle_1 \otimes |n_{L-1}^{\rm c}, n_{L-1}^{\rm a}\rangle_2 \otimes \cdots \otimes |n_1^{\rm c}, n_1^{\rm a}\rangle_L$ of state $|\mathbf{n}\rangle$, the corresponding quantity $N_{\rm e}^{\rm c\prime} + N_{\rm o}^{\rm a\prime} = N_1' = N_2 \in$ even, the same result can be obtained $\Gamma|\mathbf{n}'\rangle = |\mathbf{n}'\rangle$

When $N_1 \in$ odd, $N_{\rm e}^{\rm c} \in$ even, and $N_{\rm o}^{\rm a} \in$ odd, the number of atomic ground states is $N - N_{\rm o}^{\rm a}$ (odd) for the odd number of the lattice sites. Thus, $\Gamma|\mathbf{n}\rangle = e^{i\pi N_{\rm e}^{\rm c}}(-1)^{N-N_{\rm o}^{\rm a}} \prod_i |n_i, e(g)\rangle_i = -|\mathbf{n}\rangle$. When $N_1 \in$ odd, we can also get $N_{\rm e}^{\rm c} \in$ odd and $N_{\rm o}^{\rm a} \in$ even, $\Gamma|\mathbf{n}\rangle = -|\mathbf{n}\rangle$.

The quantity $N_1' = N_2 \in$ odd for the reflective symmetric state $P|\mathbf{n}\rangle = |\mathbf{n}'\rangle$ of state $|\mathbf{n}\rangle$, and the same result can be obtained for $\Gamma|\mathbf{n}'\rangle = -|\mathbf{n}'\rangle$.

So, for an eigenstate $|n\rangle = \Sigma_i^{\mathcal{D}}\psi_i|\mathbf{n}\rangle_i$, there is

$$P\Gamma|n\rangle = P\Sigma_i^{\mathcal{D}}(\pm)\psi_i|\mathbf{n}\rangle_i = \Sigma_i^{\mathcal{D}}(\pm)\psi_i|\mathbf{n}'\rangle_i,$$
$$\Gamma P|n\rangle = \Gamma\Sigma_i^{\mathcal{D}}\psi_i|\mathbf{n}'\rangle_i = \Sigma_i^{\mathcal{D}}(\pm)\psi_i|\mathbf{n}'\rangle_i.$$

This means that the two operators are commutative $[P, \Gamma] = 0$ and have common eigenstates and eigenvalues.

On the other hand, for $N \in$ odd,

$$\begin{matrix} N_1 \in \text{even}, \\ N_2 \in \text{odd}, \end{matrix} \quad \text{or} \quad \begin{matrix} N_1 \in \text{odd}, \\ N_2 \in \text{even}. \end{matrix}$$

When $N_1 \in$ even, $N_{\rm e}^{\rm c} \in$ odd, and $N_{\rm o}^{\rm a} \in$ odd, since the relation $L = 2N$, the number of atomic ground states is $N - N_{\rm o}^{\rm a}$ (even) for the odd number of lattice sites. Thus, $\Gamma|\mathbf{n}\rangle = e^{i\pi N_{\rm e}^{\rm c}}(-1)^{N-N_{\rm o}^{\rm a}} \prod_i |n_i^{\rm c}, n_i^{\rm a}\rangle_i = -|\mathbf{n}\rangle$. When $N_1 \in$ even, $N_{\rm e}^{\rm c} \in$ even, and $N_{\rm o}^{\rm a} \in$ even, we can also get $\Gamma|\mathbf{n}\rangle = -|\mathbf{n}\rangle$.

The quantity $N_1' = N_2 \in$ odd for the reflective symmetric state $|\mathbf{n}'\rangle$ of state $|\mathbf{n}\rangle$; as for $N_{\rm e}^{\rm c} \in$ even and $N_{\rm o}^{\rm a} \in$ odd, the number of atomic ground states is $N - N_{\rm o}^{\rm a}$ (even) for the odd number of the lattice sites. Thus, $\Gamma|\mathbf{n}\rangle = e^{i\pi N_{\rm e}^{\rm c}}(-1)^{N-N_{\rm o}^{\rm a}} \prod_i |n_i^{\rm a}, n_i^{\rm a}\rangle_i = |\mathbf{n}\rangle$, while for $N_{\rm e}^{\rm c} \in$ odd and $N_{\rm o}^{\rm a} \in$ even, we also can obtain $\Gamma|\mathbf{n}'\rangle = |\mathbf{n}'\rangle$.

When $N_1 \in$ odd, we can also get $\Gamma|\mathbf{n}\rangle = |\mathbf{n}\rangle$. The quantity $N_1' = N_2 \in$ odd for the reflective symmetric state $P|\mathbf{n}\rangle = |\mathbf{n}\prime\rangle$ of state $|\mathbf{n}\rangle$, and the same can be obtained for $\Gamma|\mathbf{n}'\rangle = -|\mathbf{n}'\rangle$.

So, for a eigenstate $|n\rangle = \Sigma_i^{\mathcal{D}}\psi_i|\mathbf{n}\rangle_i$, there is

$$P\Gamma|n\rangle = P\Sigma_i^{\mathcal{D}}(\pm)\psi_i|\mathbf{n}\rangle_i = \Sigma_i^{\mathcal{D}}(\pm)\psi_i|\mathbf{n}'\rangle_i,$$
$$\Gamma P|n\rangle = \Gamma\Sigma_i^{\mathcal{D}}\psi_i|\mathbf{n}'\rangle_i = \Sigma_i^{\mathcal{D}}(\mp)\psi_i|\mathbf{n}'\rangle_i.$$

This means that the two operators are commutative $[P, \Gamma] \neq 0$ without common eigenstates and eigenvalues.

[1] R. Nandkishore and D. A. Huse, Annu. Rev. Condens. Matter Phys. **6**, 15 (2015).

[2] D. A. Abanin, E. Altman, I. Bloch, and M. Serbyn, Rev. Mod. Phys. **91**, 021001 (2019).

[3] J. Z. Imbrie, V. Ros, and A. Scardicchio, Ann. Phys. **529**, 1600278 (2017).

[4] I. V. Gornyi, A. D. Mirlin, and D. G. Polyakov, Phys. Rev. Lett. **95**, 206603 (2005).

[5] D. M. Basko, I. L. Aleiner, and B. L. Altshuler, Ann. Phys. **321**, 1126 (2006).

[6] A. Pal and D. A. Huse, Phys. Rev. B **82**, 174411 (2010).

[7] M. Serbyn, Z. Papić, and D. A. Abanin, Phys. Rev. Lett. **110**, 260601 (2013).

[8] M. Serbyn, Z. Papić, and D. A. Abanin, Phys. Rev. Lett. **111**, 127201 (2013).

[9] M. Serbyn, Z. Papić, and D. A. Abanin, Phys. Rev. B **90**, 174302 (2014).

[10] D. A. Huse, R. Nandkishore, and V. Oganesyan, Phys. Rev. B **90**, 174202 (2014).

[11] M. Serbyn, Z. Papić, and D. A. Abanin, Phys. Rev. X **5**, 041047 (2015).

[12] M. Serbyn, A. A. Michailidis, D. A. Abanin, and Z. Papić, Phys. Rev. Lett. **117**, 160601 (2016).

[13] M. Serbyn, Z. Papić, and D. A. Abanin, Phys. Rev. B **96**, 104201 (2017).

[14] B. Bauer and C. Nayak, J. Stat. Mech.: Theory Exp. (2013) P09005.

[15] D. A. Huse, R. Nandkishore, V. Oganesyan, A. Pal, and S. L. Sondhi, Phys. Rev. B **88**, 014206 (2013).

[16] S. A. Parameswaran and R. Vasseur, Rep. Prog. Phys. **81**, 082501 (2018).

[17] A. Chandran, V. Khemani, C. R. Laumann, and S. L. Sondhi, Phys. Rev. B **89**, 144201 (2014).

[18] J. A. Kjäll, J. H. Bardarson, and F. Pollmann, Phys. Rev. Lett. **113**, 107204 (2014).

[19] D. Pekker, G. Refael, E. Altman, E. Demler, and V. Oganesyan, Phys. Rev. X **4**, 011052 (2014).

[20] F. Alet and N. Laflorencie, C. R. Phys. **19**, 498 (2018).

[21] M. Rigol, V. Dunjko, and M. Olshanii, Nature (London) **452**, 854 (2008).
[22] M. Rigol, Phys. Rev. Lett. **103**, 100403 (2009).
[23] S. Sorg, L. Vidmar, L. Pollet, and F. Heidrich-Meisner, Phys. Rev. A **90**, 033606 (2014).
[24] M. Rigol, Phys. Rev. A **80**, 053607 (2009).
[25] D. Jansen, J. Stolpp, L. Vidmar, and F. Heidrich-Meisner, Phys. Rev. B **99**, 155130 (2019).
[26] R. Mondaini, K. R. Fratus, M. Srednicki, and M. Rigol, Phys. Rev. E **93**, 032104 (2016).
[27] R. Steinigeweg, J. Herbrych, and P. Prelovšek, Phys. Rev. E **87**, 012118 (2013).
[28] W. Beugeling, R. Moessner, and M. Haque, Phys. Rev. E **89**, 042112 (2014).
[29] H. Kim, T. N. Ikeda, and D. A. Huse, Phys. Rev. E **90**, 052105 (2014).
[30] T. Yoshizawa, E. Iyoda, and T. Sagawa, Phys. Rev. Lett. **120**, 200604 (2018).
[31] E. Khatami, G. Pupillo, M. Srednicki, and M. Rigol, Phys. Rev. Lett. **111**, 050403 (2013).
[32] R. Mondaini and M. Rigol, Phys. Rev. E **96**, 012157 (2017).
[33] L. F. Santos and M. Rigol, Phys. Rev. E **82**, 031130 (2010).
[34] R. Steinigeweg, A. Khodja, H. Niemeyer, C. Gogolin, and J. Gemmer, Phys. Rev. Lett. **112**, 130403 (2014).
[35] I. M. Khaymovich, M. Haque, and P. A. McClarty, Phys. Rev. Lett. **122**, 070601 (2019).
[36] M. Mierzejewski and L. Vidmar, Phys. Rev. Lett. **124**, 040603 (2020).
[37] M. J. Hartmann, F. G. S. L. Brandão, and M. B. Plenio, Laser Photonics Rev. **2**, 527 (2008).
[38] A. D. Greentree, C. Tahan, J. H. Cole, and L. C. Hollenberg, Nat. Phys. **2**, 856 (2006).
[39] Q. Li, J.-L. Ma, T. Huang, L. Tan, H.-Q. Gu, and W.-M. Liu, Europhys. Lett. **134**, 20007 (2021).
[40] Q. Li, J.-L. Ma, and L. Tan, Phys. Scr. T **96**, 125709 (2021).
[41] D. Rossini, M. Carrega, M. Calvanese Strinati, and L. Mazza, Phys. Rev. B **99**, 085113 (2019).
[42] C. Danieli, J. D. Bodyfelt, and S. Flach, Phys. Rev. B **91**, 235134 (2015).
[43] C. Noh and D. G. Angelakis, Rep. Prog. Phys. **80**, 016401 (2017).
[44] N. Y. Yao, C. R. Laumann, J. I. Cirac, M. D. Lukin, and J. E. Moore, Phys. Rev. Lett. **117**, 240601 (2016).
[45] J. Marino, M. Eckstein, M. S. Foster, and A. M. Rey, Rep. Prog. Phys. **85**, 116001 (2022).
[46] E. Mascarenhas, L. Heaney, M. C. O. Aguiar, and M. F. Santos, New J. Phys. **14**, 043033 (2012).
[47] A. Ghoshal, S. Das, A. Sen(De), and U. Sen, Phys. Rev. A **101**, 053805 (2020).
[48] K. Pohlmeyer, Commun. Math. Phys. **46**, 207 (1976).
[49] J.-L. Ma, Q. Li, and L. Tan, Phys. Rev. B **105**, 165432 (2022).
[50] Y. Y. Atas, E. Bogomolny, O. Giraud, and G. Roux, Phys. Rev. Lett. **110**, 084101 (2013).
[51] V. Oganesyan and D. A. Huse, Phys. Rev. B **75**, 155111 (2007).
[52] C. R. Laumann, A. Pal, and A. Scardicchio, Phys. Rev. Lett. **113**, 200405 (2014).
[53] S. Johri, R. Nandkishore, and R. N. Bhatt, Phys. Rev. Lett. **114**, 117401 (2015).
[54] E. Bianchi, L. Hackl, M. Kieburg, M. Rigol, and L. Vidmar, PRX Quantum **3**, 030201 (2022).
[55] D. N. Page, Phys. Rev. Lett. **71**, 1291 (1993).
[56] V. Khemani, D. N. Sheng, and D. A. Huse, Phys. Rev. Lett. **119**, 075702 (2017).
[57] V. Khemani, S. P. Lim, D. N. Sheng, and D. A. Huse, Phys. Rev. X **7**, 021013 (2017).
[58] M. Žnidarič, T. Prosen, and P. Prelovšek, Phys. Rev. B **77**, 064426 (2008).
[59] J. H. Bardarson, F. Pollmann, and J. E. Moore, Phys. Rev. Lett. **109**, 017202 (2012).
[60] Y. Zhao, R. Narayanan, and J. Cho, Phys. Rev. B **102**, 094201 (2020).
[61] T. Mori, T. N. Ikeda, E. Kaminishi, and M. Ueda, J. Phys. B: At. Mol. Opt. Phys. **51**, 112001 (2018).
[62] B. Bertini, F. H. L. Essler, S. Groha, and N. J. Robinson, Phys. Rev. Lett. **115**, 180601 (2015).
[63] L. D'Alessio, Y. Kafri, A. Polkovnikov, and M. Rigol, Adv. Phys. **65**, 239 (2016).
[64] M. Srednicki, J. Phys. A: Math. Gen. **32**, 1163 (1999).
[65] J. M. Deutsch, Phys. Rev. A **43**, 2046 (1991).
[66] M. Srednicki, Phys. Rev. E **50**, 888 (1994).
[67] T. LeBlond, K. Mallayya, L. Vidmar, and M. Rigol, Phys. Rev. E **100**, 062134 (2019).
[68] M. Brenes, T. LeBlond, J. Goold, and M. Rigol, Phys. Rev. Lett. **125**, 070605 (2020).
[69] M. Brenes, J. Goold, and M. Rigol, Phys. Rev. B **102**, 075127 (2020).
[70] D. J. Luitz and Y. Bar Lev, Phys. Rev. Lett. **117**, 170404 (2016).
[71] K. Mallayya and M. Rigol, Phys. Rev. Lett. **123**, 240603 (2019).
[72] S. Aravinda, S. A. Rather, and A. Lakshminarayan, Phys. Rev. Res. **3**, 043034 (2021).
[73] T. LeBlond and M. Rigol, Phys. Rev. E **102**, 062113 (2020).